



Effect of stator winding chording on the performance of five phase synchronous reluctance motor

Gideon David Umoh 


Maritime Academy, Electrical Engineering Department, Oron, Akwa Ibom State, Nigeria, gideon.umoh.pg63327@unn.edu.ng

Desmond Obinna Obe 

James Cook University, College of Science and Engineering, Queensland, Australia, desmond.obe.176511@unn.edu.ng

Benjamin Okwudilili Mama 

University of Nigeria, Civil Engineering Department, Nsukka, Enugu State, Nigeria, benjamin.mama@unn.edu.ng

Pauline Ijeoma Obe * 


University of Nigeria, Industrial Technical Education Department, Nsukka, Enugu State, Nigeria, pauline.obe@unn.edu.ng

Chikodili Helen Ugwuishiwu 

University of Nigeria, Computer Science Department, Nsukka, Enugu State – Nigeria, chikodili.ugwuishiwu@unn.edu.ng

Hyacinth Agozie Eneh 

University of Nigeria, Computer Science Department, Nsukka, Enugu State – Nigeria, agozie@unn.edu.ng

Emeka Simon Obe 

Botswana International University, Electrical, Computer and Telecommunications Engineering Department, Palapye, Botswana, obe@biust.ac.bw

Submitted: 25.02.2023

Accepted: 01.12.2023

Published: 31.03.2024



* Corresponding Author

Abstract: The effect of winding chording on five-phase synchronous reluctance motor (SRM) modelled in phase variables is presented. The stator winding configuration is shifted a pole pitch from a full-pitch configuration to a 54 degrees over-full-pitched configuration incorporating the effect of 3rd harmonic of the air-gap magneto-motive force in the inductance equations. The models are monitored on starting, synchronism, loading, faults and loss of synchronism. These are considered simultaneously with vector potential, rotor speed, air-gap flux linkage and winding current. The phase variable (analytical) models have been simulated by using MATLAB/Simulink software while ANSYS Maxwell software has been used to simulate the finite element model (FEM) of the motor for corresponding chording ranges for comparison on direct online starting (DOL). Under all conditions considered in the work, the detailed results are presented and very close similarity is observed between the analytical and the nearly ideal FEM model for all chording ranges and the similarity is enhanced with increase in chording angle.

Keywords: AC machines, Electromechanical device, Finite element analysis, High-phase order electric machine, Mathematical model, Rotating machines

Cite this paper as:

Umoh, G.D., Obe, D.O., Mama, B.O., Obe, P.I., Ugwuishiwu, C.H., Enh, H.A., & Obe, E.S., Effect of stator winding chording on the performance of five phase synchronous reluctance motor. *Journal of Energy Systems* 2024; 8(1): 11-26, DOI: 10.30521/jes.1255747

1. INTRODUCTION

The development in power electronics has contributed greatly to the development of efficient electric machines. Despite the contributions of power electronics, the efficiency of electric machines can still be improved with optimize geometry and winding configuration design for direct online (DOL) starting machines. The synchronous reluctance motor (SRM), having reduced losses due to the absence of rotor winding, can be modelled for direct-on-line starting [1,2] by using a cage in the rotor and a suited winding configuration to enhance efficiency. The SRM seeks to improve the saliency of the machine when considering the geometry design, thus enhancing the reluctance torque [3,4]. Many researchers have contributed greatly to the improvement of the saliency of the machine [3-8]. To minimize the harmonics, the winding configuration is modelled to suit the supply voltage, as these are very essential for the multi-phase machine. The utilization of the multi-phase machines helps in the reduction of torque pulsation as compared to the three-phase machine [9-13]. The recognition of the direct phase variable (DPV) model when considering analysis of machine performance during faults and unbalanced conditions cannot be ignored [4,14]. The DPV model accounts for harmonics and even the rotor d - q windings of the machine, without transformation to a fictitious reference axis.

The Finite Element Method (FEM) has become a household name in electric machine design and analysis both in the academia and the industry [4, 14-22], aided in design optimization, in geometry, windings, drives system, stress analysis and temperature considerations with minimal error margin. The use of the high-order phase machines has yielded a torque enhancement with a negligible rise in copper loss because lower order harmonics could add to the fundamental component of mmf [10,23]. Five-phase machines have a lower torque pulsation than a corresponding three-phase machine [23] and this benefit manifests very much in SRMs. The five-phase machine has the ability to utilize the fundamental and third-harmonics of the air-gap MMF for torque, and is more capable of loss of phase (fault) tolerance when compared to a three-phase machine. Even though higher phase machine, other than the five-phase machine may look attractive, so also a recorded increase in the number of switching devices as well as the cost [10,12,13]. With consideration to the suppression of certain harmonics in the phase EMF and MMF, chording in both integral and fractional windings are encouraged [24-26].

This study analyses chorded stator winding of five-phase SRM from a full-pitched (FP) to over-full pitched (OFP) configurations considering the machine characteristic performance under normal, loaded, faulty and unbalanced conditions. In this paper, a detailed DPV model was used in the analysis incorporating all the winding, slot openings and rotor geometrical effects without using the simplified sinusoidal or d - q models. The finite element analysis (FEA) was used to validate the models, while considering the effect of chording ranges.

2. ANALYTICAL (PHASE-VARIABLE) MODEL OF THE FIVE PHASE SYNCHRONOUS RELUCTANCE MOTOR

A five-phase (5-ph) SRM having a cage rotor was modelled using phase variable method. Beginning with the classical volt-ampere relationship of a mutually coupled coil [4] in a rotating magnetic field:

$$V = IR + \frac{d}{dt}(LI) \quad (1)$$

The voltage equation for the five-phase SRM can be resolved to:

$$\frac{dI_I}{dt} = (L(\theta_r))^{-1} \left(V_V - \left\{ R_{rs} + \omega_r \left[\frac{d(L(\theta_r))}{d\theta_r} \right] \right\} I_I \right) \quad (2)$$

$$\omega_r = \frac{d\theta_r}{dt} \quad (3)$$

$$I_I = [i_{sa}; i_{sb}; i_{sc}; i_{sd}; i_{se}; i_{rq}; i_{rd}] \quad (4)$$

$$V_V = [v_{sa}; v_{sb}; v_{sc}; v_{sd}; v_{se}; v_{rq}; v_{rd}] \quad (5)$$

where I_I is the machine current given in Eq. (4) and V_V is voltage matrix given in Eq. (5). R_{rs} is the resistance matrix of the machine. Wherever it appears, θ_r is the rotor position. The dependence of inductances on rotor position will not be eliminated by the usual d-q transformation as this will entail the discontinuation of the use of the harmonics in the analysis.

The combined matrix of inductances of the machine consisting the stator and the rotor is given in Eq. (6).

$$L(\theta_r) = \begin{bmatrix} L_{ss} & L'_{sr} \\ \frac{2}{5}(L'_{sr})^T & L'_r \end{bmatrix} \quad (6)$$

In Eq. (6), L_{ss} and L'_{rr} , are the inductances of the stator and the rotor respectively while L'_{sr} is the stator to rotor mutual inductance. L'_{lrq} and L'_{lrd} are the leakage inductances in the q - and d -axis respectively. The electromagnetic torque is given in Eq. (7):

$$T_e = \frac{p}{2} \left(\frac{1}{2} I_{ss}^T \frac{\partial(L_{ss}(\theta_r))}{\partial\theta_r} I_{ss} + I_{ss}^T \frac{\partial(L_{sr}(\theta_r))}{\partial\theta_r} I_{rr} \right) \quad (7)$$

$$I_{ss} = [i_{sa}, \quad i_{sb}, \quad i_{sc}, \quad i_{sd}, i_{se}]^T \quad (8)$$

$$I_{rr} = [i_{rq}, \quad i_{rd}]^T \quad (9)$$

In terms of mechanical quantities, the torque can be written as:

$$T_e = J \left(\frac{p}{2} \right) \frac{d\omega_r}{dt} + T_l \quad (10)$$

Here I_{ss} and I_{rr} are the stator and rotor current matrices respectively while J is the polar moment of inertia (kgm^2), p is the number of magnetic poles while T_l is the load torque (N m).

The stator winding resistance R_S can be calculated from Eq. (11).

$$R_S = \frac{l_x}{a_c \sigma_c} \quad (11)$$

In Eq. (11), σ_c is the conductivity, l_x is the length and a_c is the conductor cross-sectional area. The total length of the conductor is given in Eq. (12).

$$l_x = \frac{v_{xl}}{a_c} \quad (12)$$

Where v_{xl} is the total volume of conductors per machine phase, the slot conductor's volume v_{xs} and the end turn volume v_{xe} are given in Eq. (13), Eq. (14) and Eq. (15), respectively.

$$v_{xl} = v_{xs} + 2v_{xe} \quad (13)$$

$$v_{xs} = (l + 2e)a_c \sum_{i=1}^{s_y} |N_{x,i}| \quad (14)$$

$$v_{xe} = \frac{2\pi}{s_y} \bar{r}_x a_c E_x \quad (15)$$

e , $\frac{2\pi}{s_y}$, E_x , \bar{r}_x , N_x and s_y are the axial length from the end of the machine lamination to the centre for the end-turn bundle, angle of the end conductor sector, end connector sector length, total number of conductors and the number of slots respectively.

For the different models, change in volume is only recorded with the end turn volume since the chording does not actually change the volume of the slot conductors. To accommodate the changes across the models, $x_i E_k$ is introduced as in Eq. (16)

$$v_{xe} = \frac{2\pi}{s_y} \bar{r}_x a_c x_i E_k \quad (16)$$

where E_k is a constant term for the end connector sector length, while x_i represent the change in sector length across the model for i_{th} model.

3. CONFIGURATIONS (MODELS) OF THE MACHINE UNDER STUDY

In this paper, four configurations, termed models are considered for the purpose of analysis. The five-phase SRM stator is wound as full-pitched, over-full-pitched 18 degrees chording, over-full-pitched 36 degrees chording and over-full-pitched 54 degrees chording and represented as Models I to IV in Table 1 showing only for one pole for brevity. These models also offer a negligible variation in the length of the windings and end connections.

Table 1: Five-phase four-pole winding configuration.

Slots	Model I		Model II		Model III		Model IV	
	Full-pitched		Over-full pitched 18 deg.		Over-full pitched 36 deg.		Over-full pitched 54 deg.	
	L1	L2	L1	L2	L1	L2	L1	L2
1	A ⁺	A ⁺	A ⁺	D ⁻	A ⁺	D ⁻	A ⁺	B ⁺
2	A ⁺	A ⁺	A ⁺	A ⁺	A ⁺	D ⁻	A ⁺	D ⁻
3	C ⁻	C ⁻	C ⁻	A ⁺	C ⁻	A ⁺	C ⁻	D ⁻
4	C ⁻	C ⁻	C ⁻	C ⁻	C ⁻	A ⁺	C ⁻	A ⁺
5	E ⁺	E ⁺	E ⁺	C ⁻	E ⁺	C ⁻	E ⁺	A ⁺
6	E ⁺	E ⁺	E ⁺	E ⁺	E ⁺	C ⁻	E ⁺	C ⁻
7	B ⁻	B ⁻	B ⁻	E ⁺	B ⁻	E ⁺	B ⁻	C ⁻
8	B ⁻	B ⁻	B ⁻	B ⁻	B ⁻	E ⁺	B ⁻	E ⁺
9	D ⁺	D ⁺	D ⁺	B ⁻	D ⁺	B ⁻	D ⁺	E ⁺
10	D ⁺	D ⁺	D ⁺	D ⁺	D ⁺	B ⁻	D ⁺	B ⁻

Legend: L1 – Layer 1, L2 – Layer 2

4. INDUCTANCE CALCULATION

For the purpose of analysis, an approximation can be made on the winding expression by limiting it to only the fundamental and the 3rd harmonic constituents for each phases together with their corresponding phase shifts. Each phase winding function for any typical phase will be of the form:

$$N_b(\varnothing_s) = \frac{4N}{\pi 2} \left[k_{w1} \cos(\varnothing_s + \alpha) - \frac{1}{3} k_{w3} \cos(3(\varnothing_s + \alpha)) \right] \quad (17)$$

In Eq. (17), $k_{w1} = k_{c1}k_{d1}$, $k_{w3} = k_{c3}k_{d3}$; wherein k_{cn} and k_{dn} are the chording and the distribution factor of the nth harmonics. α is $0, -\frac{2\pi}{5}, -\frac{4\pi}{5}, \frac{4\pi}{5}, \frac{2\pi}{5}$ for phases A to E respectively, while \varnothing_s is the stator angular position. To find any inductance expression, we use:

$$L_{xy} = \mu_0 r l \int_0^{2\pi} N_x(\varphi) N_y(\varphi) g^{-1}(\varphi, \theta_r) d\varphi \quad (18)$$

In Eq. (18), $N_x(\varphi)$ and $N_y(\varphi)$ are the winding functions of phases X and Y respectively. $g^{-1}(\varphi, \theta_r)$ is the inverse air gap function while l is the axial length of the air gap, r is the radius to the mean of the air gap and μ_0 is the permittivity of free space. The inverse air-gap function including the 3rd harmonic component is given in Eq. (19).

$$g^{-1}(\varnothing_s, \theta_r) = a - b \cos 2(\varnothing_s - \theta_r) + \frac{b}{3} \cos 6(\varnothing_s - \theta_r), \quad (19)$$

where,

$$a = \frac{1}{2} \left(\frac{1}{g_a} + \frac{1}{g_b} \right) \quad (20)$$

$$b = \frac{2}{\pi} \left(\frac{1}{g_a} - \frac{1}{g_b} \right) \sin \pi \beta \quad (21)$$

In Eqs. (20) and (21), g_a the air gap at pole face, g_b is the airgap between the poles and β is the pole arc/pole pitch ratio.

5. SIMULATION OF THE DPV (ANALYTICAL MODEL)

The parameters of the 5-ph SRM used in the simulation of the machine are given in Table 2.

Table 2. The parameters of the 5-phase SRM.

Quantities	Value	Quantities	Value
Stator outer / inner radius	105.02 / 68.09mm	Number of poles	4
Rotor radius	67.69mm	Frequency	50Hz
Effective stack length	160.22mm	Ratio pole arc / pole pitch	2/3
Number of slots	40	phase voltage V_{5ph}	370v
Number of turns	48	Rotor q-axis leakage inductance L_{lqr}	4.2mH
Main air-gap length g_a	0.4mm	Rotor d-axis leakage inductance L_{ldr}	3.5mH
Inter polar slot space g_b	21.3mm	Rotor q-axis resistance R_{qr}	0.08 Ω
Stator slot depth	18mm	Rotor d-axis resistance R_{dr}	0.52 Ω
Stator slot pitch	9 ^o	Moment of inertia J	0.0389kg/m ²

The developed machine stator winding models: Models I-IV which were modelled about a slot pitched, were studied for machine behavior at synchronism, loading, fault and the vector potential. The plots of the Finite Element Model (FEM) are shown in Figs. 2, 3 and 4 respectively, and tabulated in Table 3. A fault leading to loss of e-phase was created for a period of 0.5 s while the machine is loaded.

Table 3. Vector potential characteristics.

Models	Synchronism	Loading	Fault	% Drop on loading	% Drop at fault
Model I	19.15	18.44	18.28	3.71	0.87
Model II	18.86	17.99	17.88	3.59	0.61
Model III	19.09	18.73	18.62	1.89	0.58
Model IV	19.37	19.35	19.25	0.103	0.52

The plot of the vector potential at synchronism shows a maximum value of 19.37×10^{-3} Wb/m for model III, and a recorded 1.44 %, 2.63% and 1.14 % decreased in value for Models III, II and I respectively. This variance in the vector potential of the models is an indication of the developed potential at each of the coils in the slots. On loading, a corresponding drop in value is recorded for all the models, decreasing as the chording angle increases. A similar drop in percentage value is also experienced with the models during fault, with decreasing value as the chording angle increases. Model IV showed the least drop in value on load and during fault with a percentage drop values of 0.103 % and 0.52 % on load and during fault respectively as can be seen in Table 3.

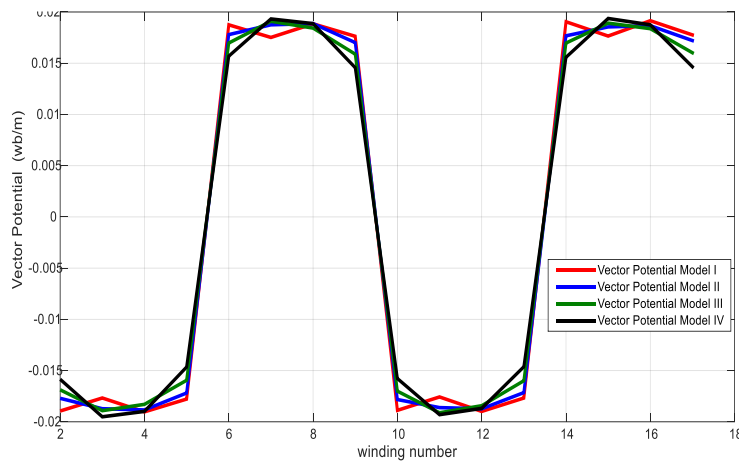


Figure 1. A-phase vector potential plot at synchronism.

The machine was loaded with a continuous duty cycle load torque of 50 N m lasting for 3.2 seconds as a step load before an additional ramp load torque was introduced, reaching a maximum torque of 110 N m at 3.5 seconds. The speed characteristics of the machine was monitored under these loading conditions as shown in Fig. 5.

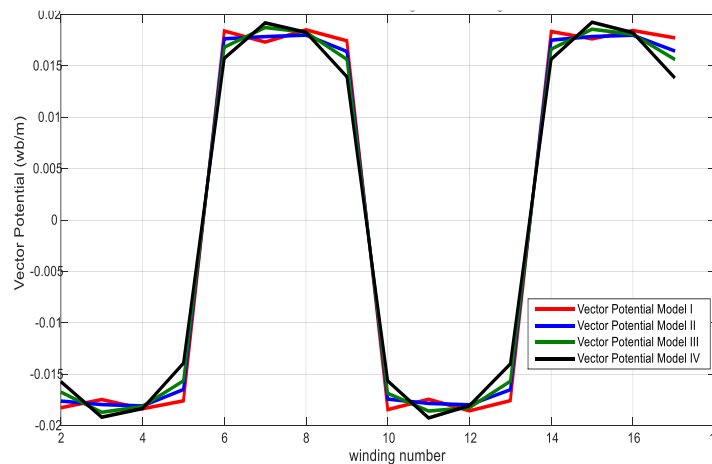


Figure 3. A-Phase Vector potential plot on Load

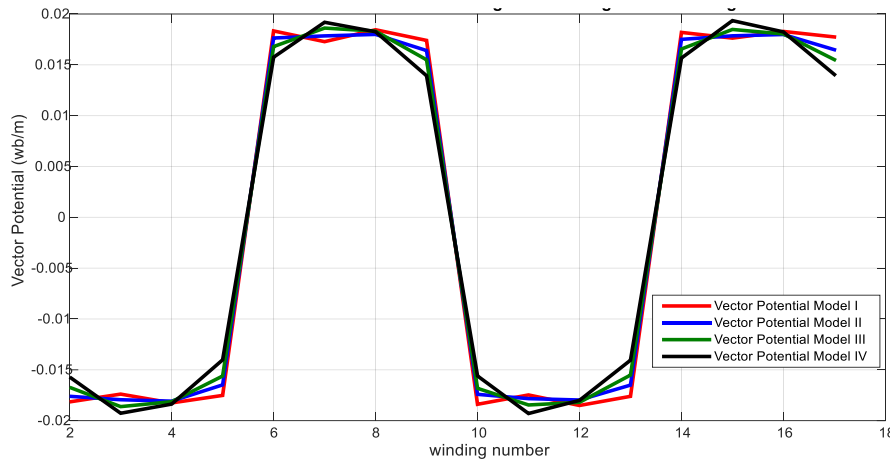


Figure 4. A-Phase Vector potential plot during fault

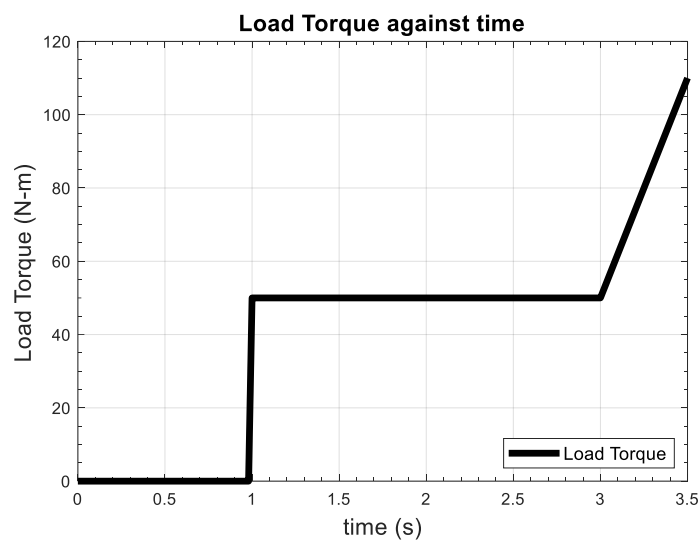


Figure 5. Plot of Load Torque against time

The machine was loaded with a continuous duty cycle load torque of 50N-m lasting for 3.2 seconds as a step load before an additional ramp load torque was introduced, reaching a maximum torque of 110N-m at 3.5 seconds. The speed characteristics of the machine was monitored under these loading conditions as shown in Fig. 5.

The speed characteristics for Models I to IV for FEM and DPV are presented in Figs. 6 to 9, respectively, while the speed characteristics for the DPV and the FEM are presented for all the considered models in Figs. 10 and 11, respectively. Longer settling time is observed with increase in chording at synchronism and on loading, but a decreasing settling time with increase in chording during fault. At loss of synchronism, Model IV record the greatest time for both the DPV and the FEM models, as compared to time value of 3.279 seconds, 3.141 seconds and 3.115 seconds for Models III, II and I, respectively, while a time value of 3.212 seconds, 3.191 seconds and 3.168 seconds for Models III, II and I respectively. The settling times for the speed under different conditions are shown in Table 4.

The speed transient characteristics at starting, loading, under fault and when the fault has been cleared are shown in Table 5. The speed transients at starting showed the least percentage value rise of 8.9 % about the synchronous speed for Model I as likened to a percentage rise of 10.13%, 16.40% and 23.33% for Models IV, III and II respectively for the FEM, which has a comparable lower transient rise as compared to the highest and the least percentage value rise of 31.53% and 15.27 % for Model II and Model I respectively.

Table 4. Settling time and time of loss of synchronism for the considered characteristics.

Model	Synchronism	Loading	Fault	Fault cleared	Loss of Synchronism
Finite Element Method (FEM)					
I	0.887	1.601	2.189	2.905	3.115
II	0.890	1.662	2.154	2.977	3.141
III	0.930	1.679	2.013	>3	3.279
IV	0.975	1.689	2.093	>3	3.351
Direct Phase Variable (DPV) Model					
I	0.889	1.600	2.182	2.854	3.168
II	0.901	1.664	2.177	2.925	3.191
III	0.933	1.678	2.167	2.951	3.212
IV	0.977	1.688	2.155	2.968	3.339

The speed transient when loaded showed a minimal percentage rise of 1.93% and 2.13% in Model IV for FEM and analytical models respectively. When fault occurred the percentage transient rise of 4.47 % and 6.07% were observed in Model I for analytical and FEM respectively. When the fault of e-phase loss was cleared, the percentage rise value of 2.93% and 6.27% were recorded in Model I in analytical and FEM respectively.

The FEM Speed characteristics plots showing transient for Models I, II, III, and IV at starting, loading, loss of phase fault and synchronism loss are shown in Figs. 12,13,14 and 15, respectively.

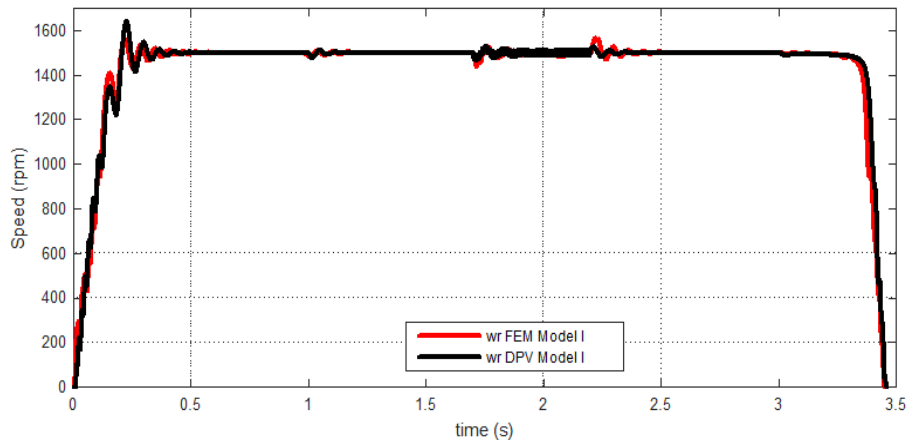


Figure 6. FEM and analytical (phase variable) plots of speed for Model I.

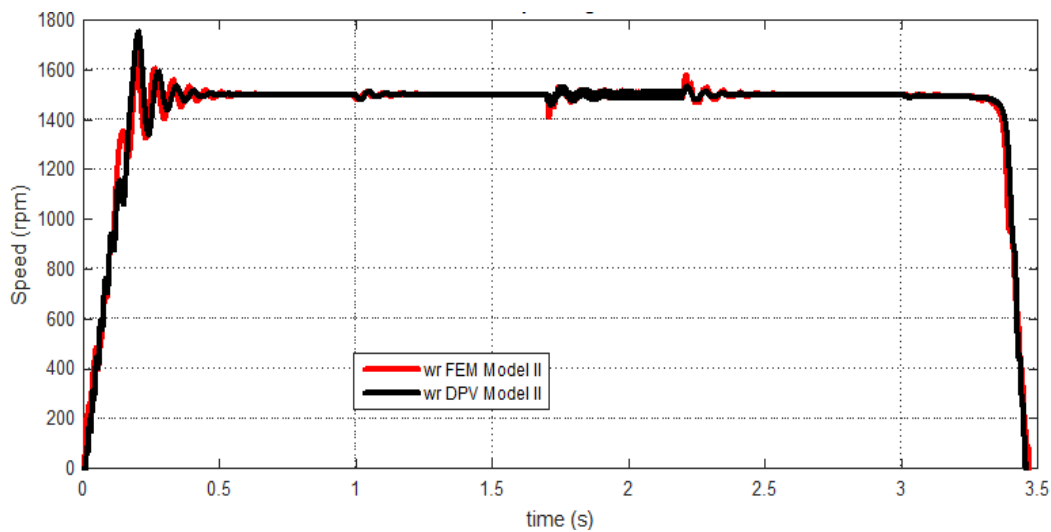


Figure 7. FEM and analytical (phase variable) plots of speed for Model II.

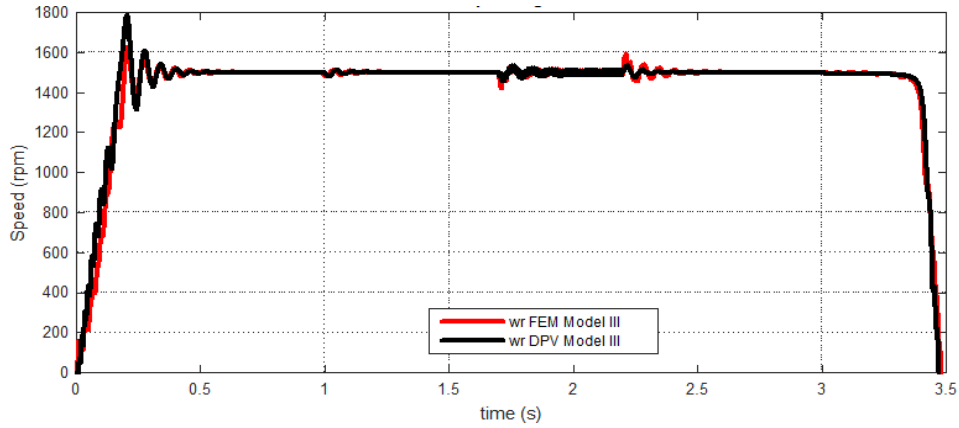


Figure 8. FEM and analytical (phase variable) plots of speed for Model III.

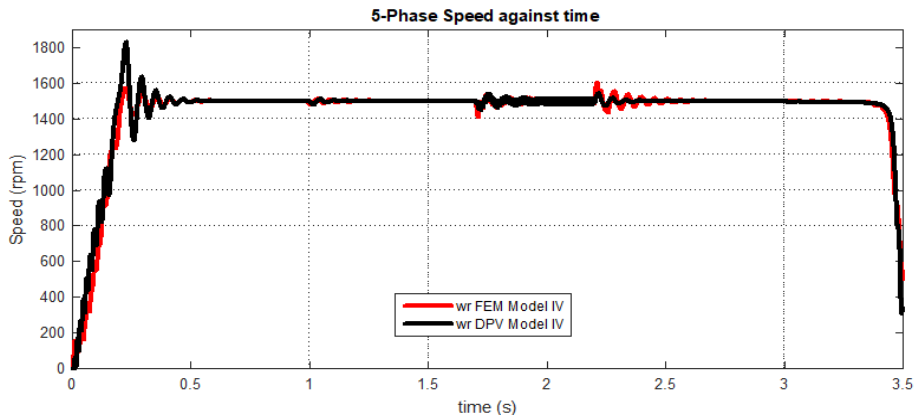


Figure 9. FEM and analytical (phase variable) plots of speed for Model IV.

Table 5. Speed performance characteristics.

Speed Transient (rpm)	Start		Loading		Fault		Fault cleared	
	Finite Element Method (FEM)							
	(max – min)	%	(max – min)	%	(max – min)	%	(max – min)	%
FP (Model I)	1564 – 1430	8.93	1512 – 1480	2.13	1528 – 1437	6.07	1564 – 1470	6.27
OFP (Model II)	1677 – 1327	23.33	1513 – 1480	2.20	1531 – 1411	8.00	1584 – 1467	7.80
OFP (Model III)	1629 – 1383	16.40	1513 – 1479	2.27	1527 – 1422	7.00	1595 – 1454	9.40
OFP (Model IV)	1577 – 1425	10.13	1512 – 1483	1.93	1535 – 1411	8.27	1603 – 1437	11.07
Direct Phase Variable (DPV) Model								
FP (Model I)	1642 – 1413	15.27	1513 – 1479	2.27	1531 – 1464	4.47	1527 – 1483	2.93
OFP (Model II)	1755 – 1340	31.53	1513 – 1449	4.27	1532 – 1460	4.80	1533 – 1479	3.60
OFP (Model III)	1789 – 1316	27.67	1513 – 1479	2.27	1534 – 1458	5.07	1536 – 1477	3.93
OFP (Model IV)	1834 – 1280	15.27	1513 – 1481	2.13	1541 – 1448	6.20	1543 – 1471	4.80

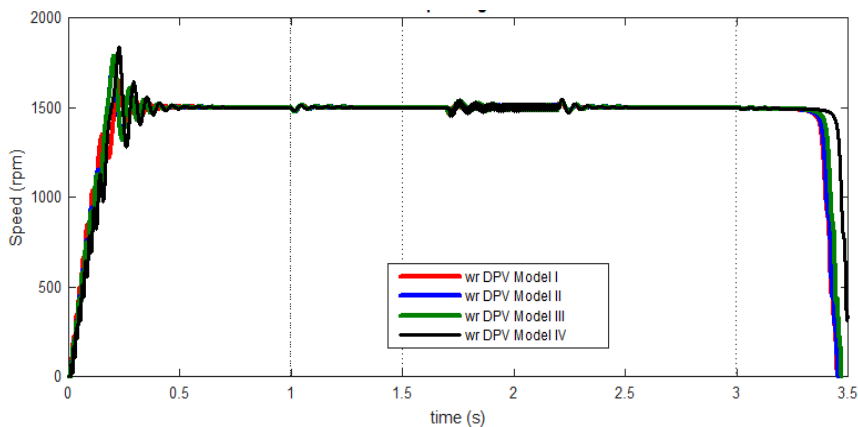


Figure 10. Comparison of speed plots for the four models using the phase variable (analytical) method.

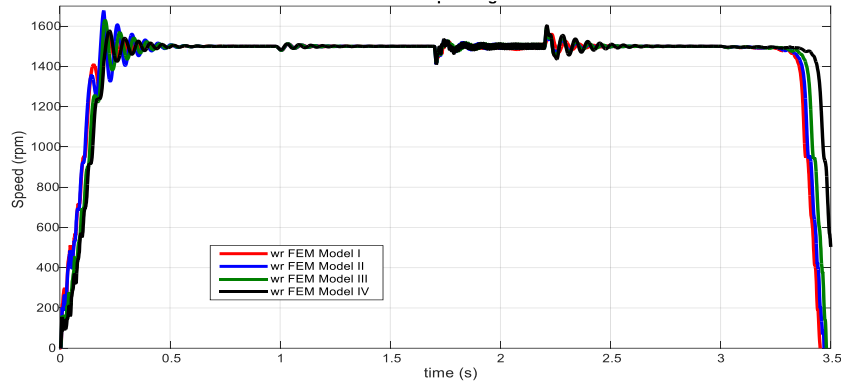


Figure 11. Comparison of Speed plots for the four models using FEM.

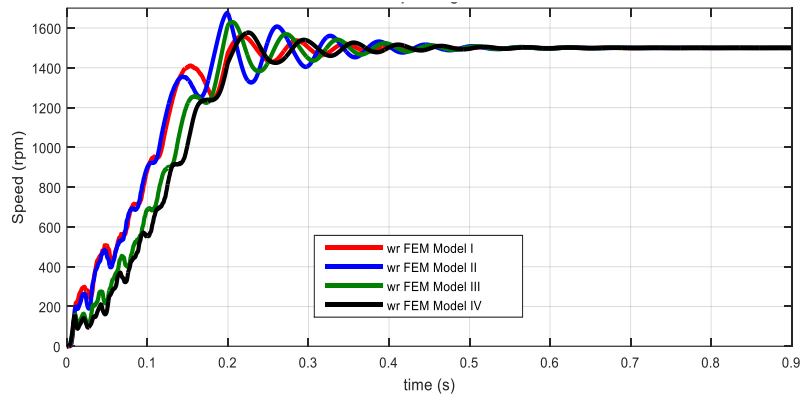


Figure 12. Speed characteristics (Showing transient at start to synchronism).

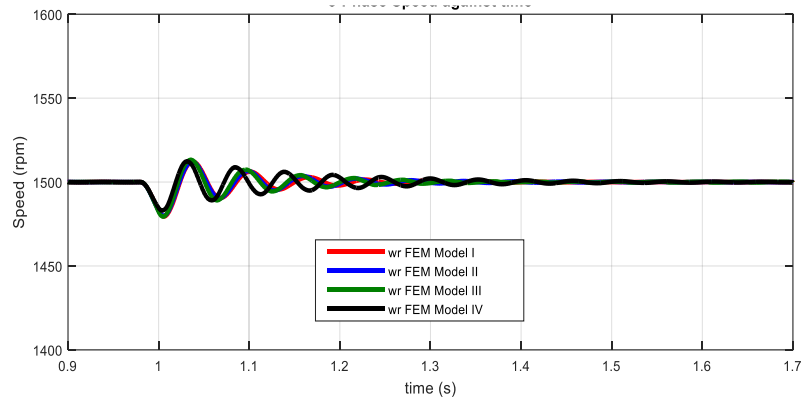


Figure 13. Speed departures (transient) at loading.

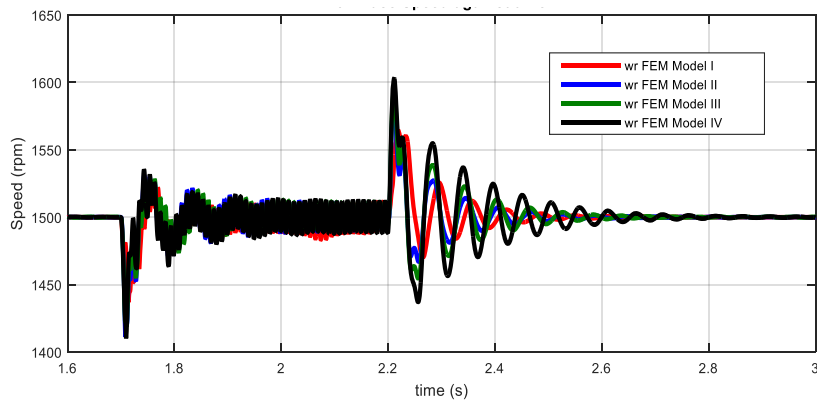


Figure 14. Speed departures (transient) following loss and successive reinstatement of e-phase.

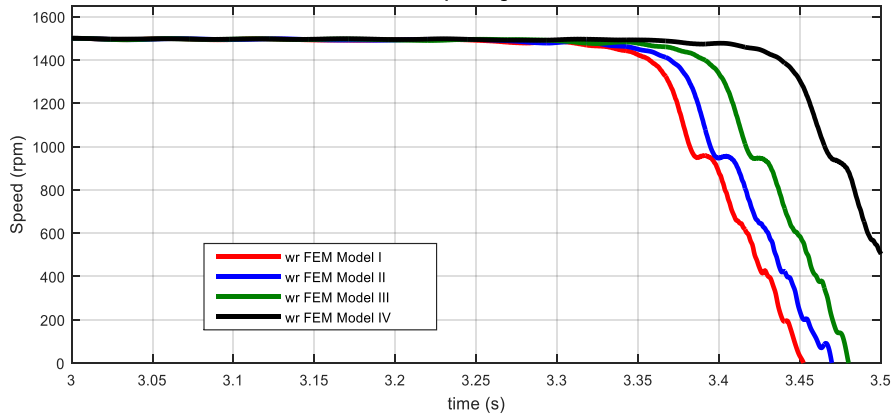


Figure 15. Loss of synchronism on loading.

The effect chording on the machine flux linkage at were monitored during synchronism, loading fault and then clearance of the fault with the FEM and the phase variable models. The result are shown in Table 6. The a-phase flux plot for all the considered models for FEM at synchronism, loading and faults are presented in Figs. 16, 17, 18 and 19, respectively. A difference of 2.43% is observed between the FEM and the DPV for Model I, while 3.47%, 5.92% and 8.03% differences are seen for Models II, III and IV between the FEM and the analytical model at synchronism, respectively. The value of the flux linkage is generally observed to decrease as the chording angle increases, and is observed in both the FEM and the analytical models as tabulated in Table 6.

Table 6. Flux linkage characteristics

Model	Synchronism	Loading	Fault	Fault cleared
	Value(±)	Value(±)	Value(Max-Min)	Value(±)
<u>Finite Element Method (FEM)</u>				
I	1.126	1.104	0.8534 -0.8537	1.105
II	1.112	1.087	0.8417 -0.8429	1.088
III	1.081	1.064	0.7882 -0.7881	1.065
IV	1.054	1.034	0.7684 -0.7692	1.032
<u>Direct Phase Variable (DPV) Model</u>				
I	1.154	1.146	1.117 -1.144	1.145
II	1.152	1.143	1.112 -1.143	1.143
III	1.149	1.138	1.107 -1.139	1.140
IV	1.146	1.133	1.100 -1.135	1.135

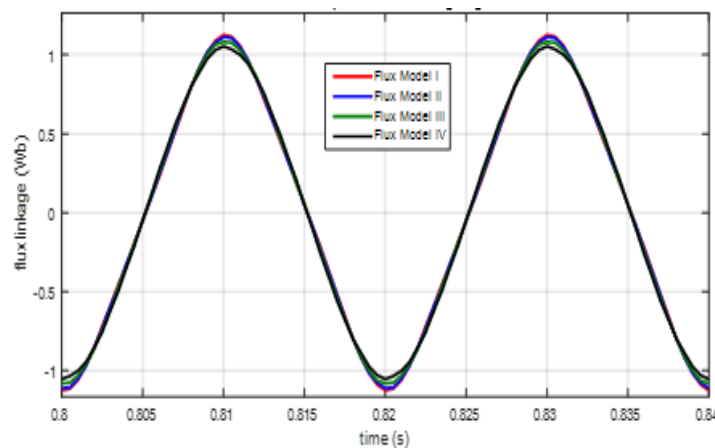


Figure 16. Flux Linkage characteristics for FEM (at synchronism before loading).

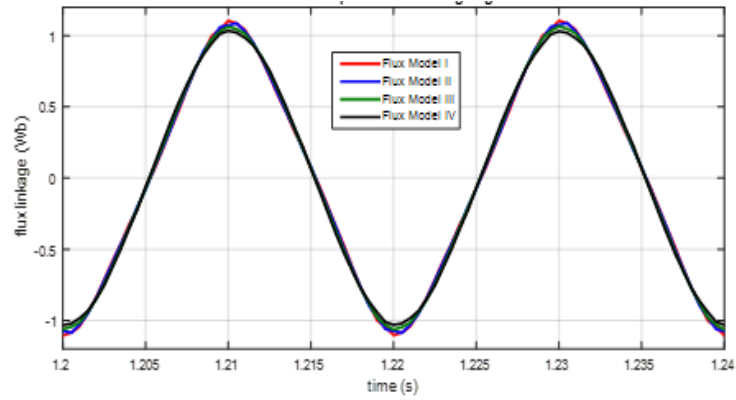


Figure 17. Flux Linkage characteristics on load for FEM (50 N m load torque).

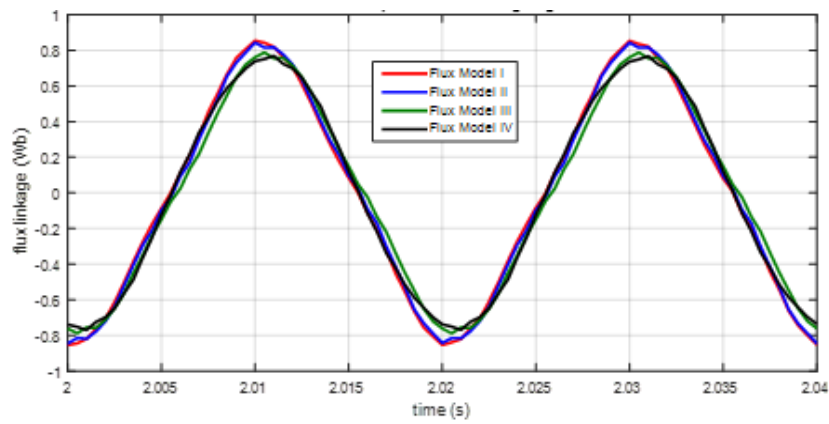


Figure 18. Flux linkage characteristics for FEM (during loss of e-phase fault).

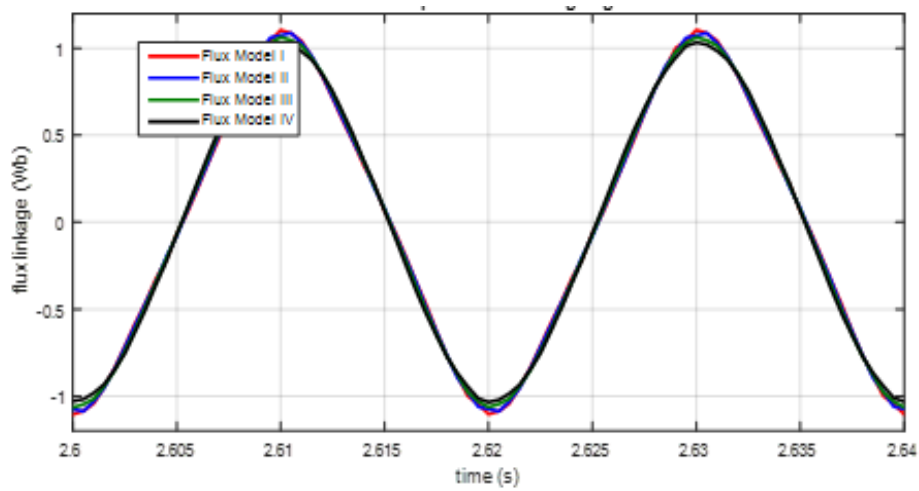


Figure 19. Flux linkage characteristics for FEM (after loss of e-phase fault is cleared).

The current plots for each of the five phases are analogous as a symmetrical winding following the application of load. Varied characteristics can be observed for the different models when the currents in phase A is presented. These are shown in Figs. 20, 21 and Table 7.

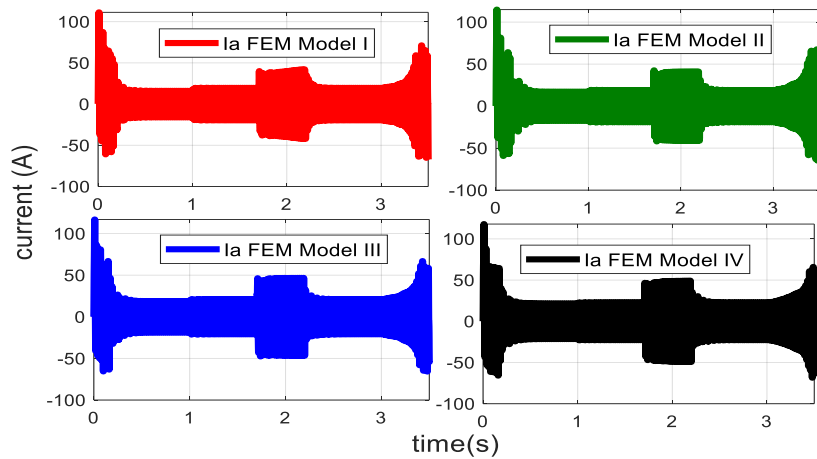


Figure 20. Current plots for FEM.

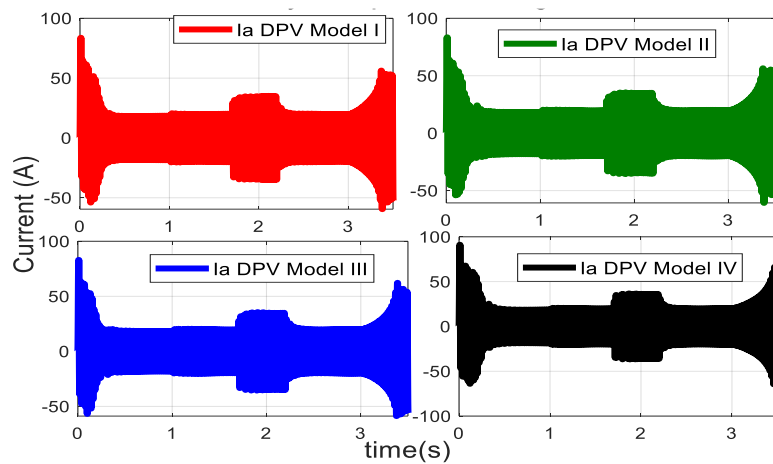


Figure 21. Current characteristics for DPV model.

During starting, a transient rise is observed in the FEM model, and particularly in Model IV with a value of 118 A as compared to other models. Similar higher transient rise in current was seen in the phase variable with a high as 91.16 A for Model IV.

At synchronism, Model IV still has the highest value of 19.41 A and 21.61 A for DPV and FEM respectively as compared to Model I, having the values of 16.56 A and 16.11 A for DPV and FEM respectively. On loading, a current rise of 15.91% and 12.88% was observed in Model I for FEM and DPV respectively, as compared to an observed Model IV current rise of 5.72% and 4.15% rise for FEM and DPV, respectively. During the fault, for Model I, a 52.16% current rise was observed for FEM as compared to a 50.54% current rise for DPV, while in Model IV, a 53.14% current rise is observed in FEM as compared to 49.61% rise for DPV.

Table 7. Phase A current performance.

<i>FEM</i>					
Model	Start Transient (max – min)	Synchronism (A)	Loading (A)	Fault (A)	Fault cleared (A)
<u>Finite Element Method (FEM)</u>					
I	111.3 – -61.15	16.11	19.16	40.05	19.11
II	114.9 – -59.34	17.23	19.73	41.14	19.73
III	116.9 – -65.64	18.89	21.01	46.61	21.02
IV	118.0 – -69.52	21.61	22.92	48.92	22.92
<u>Direct Phase Variable (DPV) Model</u>					
I	87.73 – -53.97	16.56	19.01	38.44	19.01
II	82.93 – -52.2	17.91	19.57	39.19	19.58
III	83.06 – -56.86	18.95	19.80	39.87	19.82
IV	91.16 – -64.01	19.41	20.25	40.19	20.64

Loss of synchronism occurs during ramp loading as Model IV shows a higher load carrying capacity for both the FEM and DPV with a carrying capacity of 92.06 N m and 90.62 N m respectively for Model IV. For Model I, the corresponding values are 63.74 N m and 70.16 N m. As the chording angle increases, the carrying capacity (pull-out torques) also increases as recorded for the considered models as tabulated in Table 8.

Table 8. Pull-out load torque.

Load Torque (N-m)	Loss of Synchronism	
	Torque	Time(s)
<u>Finite Element Model (FEM)</u>		
FP (Model I)	63.74	3.115
OFP 18 deg. (Model II)	67.04	3.141
OFP 36 deg. (Model III)	83.48	3.279
OFP 54 deg. (Model IV)	92.06	3.351
<u>Direct Phase Variable (DPV) Model</u>		
FP (Model I)	70.16	3.168
OFP 18 deg. (Model II)	72.86	3.191
OFP 36 deg. (Model III)	79.38	3.212
OFP 54 deg. (Model IV)	90.62	3.339

6. CONCLUSION

Comparatively, authors are aware of the multiple coupled circuit model developed by Munoz and Lipo [27] but the method is not used here because several variables are involved whereas this paper intends to provide actual results based on DPV model which can be extended to other machine variants. Accounting for chording in the stator winding, the developed model of five-phase synchronous reluctance motor has been investigated with MATLAB/Simulink and ANSYS Maxwell and compared with FEM simulations. In this study, machine performance during starting, load application, during losses of phase synchronism due to loading were considered. The behavior of the machine's vector potential, rotor speed, air-gap flux linkage, stator winding phase current and the pull-out capability for the modelled stator winding configuration of full-pitched, over full-pitched with chording angles of 18°, 36° and 54° were investigated. These models showed similar characteristics with no more than 10% deviation in value between the FEM and the DPV models.

For the flux linkages, difference of 2.43% is observed between the FEM and the DPV for Model I, while differences 3.47%, 5.92% and 8.03% are observed for Models II, III and IV, respectively between the FEM and the DPV at synchronism. The value of the flux linkage is generally observed to decrease as the chording angle increases, and is observed in both the FEM and the DPV models. On loading, a brief transient oscillation was observed, but at loss of phase fault, the machine still runs at synchronous speed with fluctuations about the synchronous speed, and is observed in all the considered models. The full pitched machine showed the minimal loading accommodation of 70.16 N m at 3.17 s for the DPV and 63.74 at 3.115 s for the FEM is recorded in Model I (full pitched) as compared to a maximum loading accommodation of 90.62 N m at 3.339 for DPV and 92.06 N m at 3.351 s for FEM in Model IV (over-full-pitched 54 degrees chording). From the above results, it is fundamentally observed that there is a very close similarity between DPV and the nearly ideal FEM model for all chording ranges thereby justifying the use of DPV model as a superior alternative to the $d-q$ model which has lots of encumbrances. It is also particularly observed that the similarity between the DPV and the FEM increases with increase in chording angle. Finally, it is pertinent to mention that all the developed models still gave enough necessary information on the analysis of five phase SRM, but based on the required application, a particular model can be adopted.

REFERENCES

- [1] Liu, HC, Lee, J. Optimum Design of an IE4 Line-Start Synchronous Reluctance Motor Considering Manufacturing Process Loss Effect. *IEEE Transactions on Industrial Electronics*, 2017; 65: 3104-3114. DOI: 10.1109/TIE.2017.2758738
- [2] Kersten, A, Liu, Y, Pehrman, D, Thiringer, T. Rotor Design of Line-Start Synchronous Reluctance Machine with Round Bars. *IEEE Transactions on Industry Applications*, 2019; 55: 3685-3696, DOI: 10.1109/TIA.2019.2914010
- [3] Ogbuka, CU, Nwosu, CM, Umoh, GD. A new cross-saturated torque model of highly utilized synchronous reluctance machine, *Archives of Electrical Engineering*. 2018; 67: 109–121, DOI: 10.24425/118995
- [4] Obe, ES, Binder, A. Direct-phase-variable model of a synchronous reluctance motor including all slot and winding harmonics. *Energy Conversion and Management*, 2011; 52: 284-291. DOI: 10.1016/j.enconman.2010.06.069
- [5] S. Stipetic, S, Zarko, D, Cavar, N. Adjustment of Rated Current and Power Factor in a Synchronous Reluctance Motor Optimally Designed for Maximum Saliency Ratio. *IEEE Transactions on Industry Applications*, 2020; 56: 2481-2490, DOI: 10.1109/TIA.2020.2971442
- [6] Jurca, FN, Inte, R, Martis, C, Optimal rotor design of novel outer rotor reluctance synchronous machine. *Electrical Engineering*, 2020; 102: 107–116, DOI: 10.1007/s00202-019-00786-w
- [7] Chai, W, Zhao, W, Kwon, B-i. Optimal Design of Wound Field Synchronous Reluctance Machines to Improve Torque by Increasing the Saliency Ratio. *IEEE Transactions on Magnetics*, 2017; 53: 1-4, DOI: 10.1109/TMAG.2017.2707459
- [8] Hrabovcová, V, Makyš, V, Rafajdus, P, Šebest, M. Improved barriers rotor of the reluctance synchronous motor. *Electrical Engineering* 2017; 99: 1325–1335, DOI: 10.1007/s00202-017-0620-5
- [9] Umesh, BS, Sivakumar, K. Pole-Phase Modulated Multiphase Induction Motor Drive with Reduced Torque Ripple and Improved DC Link Utilization. *IEEE Transactions on Power Electronics*, 2017; 32: 7862-7869, DOI: 10.1109/TPEL.2016.2634092
- [10] Parsa, L, Toliyat, HA. Five-phase interior permanent magnet motor with low torque pulsation. *IEEE Transactions on Industry Applications*, 2007; 43: 40-46, doi: 10.1109/TIA.2006.887235.
- [11] Schreier, J, Bendl, J, Chomat, M. Analysis of influence of third spatial harmonic on currents and torque of multi-phase synchronous machine with permanent magnets, *Electrical Engineering*, 2018; 100: 2095–2102. DOI: 10.1007/s00202-018-0686-8
- [12] Umoh, GD, Obe, CT, Ogbuka, CU, Ekpo, G, Obe, ES, Direct-Phase Variable Modelling and Analysis of Five-Phase Synchronous Reluctance Motor for Direct-on-Line Starting. *Przeegląd Elektrotechniczny* 2021; 97: 24-29, DOI: 10.15199/48.2020.01.21
- [13] Umoh, GD, Ogbuka, CU, Obe, ES. Modelling and Analysis of Five-Phase Permanent Magnet Synchronous Motor in Machine Variables. *Przeegląd Elektrotechniczny*, 2020; 96: 87-92, DOI: 10.15199/48.2021.01.05
- [14] Özüpak, Y. Design and Analysis of a Synchronous Generator Using Finite Element Method Based ANSYS-Maxwell. *International Journal of Engineering and Applied Sciences*, 2022; 14: 66-76, <https://doi.org/10.24107/ijeas.1163134>
- [15] Torkaman, H, Afjei, E, Gorgani, A, Faraji, N, Karim, H, Arbab, N. External rotor SRM with high torque per volume: design, analysis, and experiments. *Electrical Engineering*, 2013; 95: 393–401, DOI: 10.1007/s00202-012-0265-3
- [16] Duan, Y, Ionel, DM. A Review of Recent Developments in Electrical Machine Design Optimization Methods with a Permanent-Magnet Synchronous Motor Benchmark Study. *IEEE Transactions on Industry Applications*, 2013; 49: 1268-1275, DOI: 10.1109/TIA.2013.2252597
- [17] Epemu, A, Onyishi, D, Obe, S. Performance Analysis of Line-Start Concentrated Dual-winding Synchronous Reluctance Machine with Capacitive Assistance. *Gazi University Journal of Science*, 2022; 35: 917-934, DOI: 10.35378/gujs.887673
- [18] Krüttgen, C, Steentjes, S, Glehn, G, Hameyer, K. Parametric Homogenized Model for Inclusion of Eddy Currents and Hysteresis in 2-D Finite-Element Simulation of Electrical Machines. *IEEE Transactions on Magnetics*, 2017; 53, 1-4, DOI: 10.1109/TMAG.2017.2660460
- [19] Zhao, W, Xing, F, Wang, T, Lipo, TA, Kwon, B. Design and Analysis of a Novel PM-Assisted Synchronous Reluctance Machine with Axially Integrated Magnets by the Finite-Element Method. *IEEE Transactions on Magnetics*, vol. 53, no. 6, pp. 1-4, June 2017, Art no. 8104104, DOI: 10.1109/TMAG.2017.2662717
- [20] Tiegna, H, Bellara, A, Amara, Y, Barakat, G. Analytical Modelling of the Open-Circuit Magnetic Field in Axial Flux Permanent-Magnet Machines with Semi-Closed Slots. *IEEE Transactions on Magnetics*, 2012; 48: 1212-1226, DOI: 10.1109/TMAG.2011.2171979.
- [21] Azizi, H, Vahedi, A. Sensitivity Analysis and Optimum Design for the Stator of synchronous reluctance machine using the coupled finite and Taguchi method. *Turkish Journal of Electrical and Computer Sciences*, 2015; 23: 38-51, DOI: 10.3906/elk-1111-40.

- [22]Nekoubin A, Soltani J, Dowlatshahi, M. Comparative analysis of three-phase and five-phase permanent-magnet motor based on finite element method. *Journal of Electrical Engineering & Technology*, 2020; 15: 1705–1712, DOI: 10.1007/s42835-020-00444-3.
- [23]Pereira, LA, Scharlau, CC, Pereira, LFA, Haffner, S. Influence of Saturation on the Airgap Induction Waveform of Five-Phase Induction Machines. *IEEE Transactions on Energy Conversion*, 2012; 27: 29-41, DOI: 10.1109/TEC.2011.2169674.
- [24]Bomela, XB, Kamper, MJ. Effect of stator chording and rotor skewing on performance of reluctance synchronous machine. *IEEE Transactions on Industry Applications*, 2002; 38: 91-100, DOI: 10.1109/28.980362.
- [25]Barcaro, M, Bianchi, N, Magnussen, F. Six-Phase Supply Feasibility Using a PM Fractional-Slot Dual Winding Machine. *IEEE Transactions on Industry Applications*, 2011; 47: 2042-2050, DOI: 10.1109/TIA.2011.2161859.
- [26]Raziee, SM, Misir, O, Ponick, B. Winding Function Approach for Winding Analysis. *IEEE Transactions on Magnetics*, 2017; 53: 1-9, DOI: 10.1109/TMAG.2017.2712570.
- [27]Munoz, AR, Lipo, TA. Complex Vector Model of the Squirrel-cage Induction Machine Including Instantaneous Rotor Bar Currents, *IEEE Transactions on Industry Applications*, 1999; 35: 1332-1340, DOI: 10.1109/28.806047.